Localized photonic nanojet based sensing platform for highly efficient signal amplification and quantitative biosensing

Zhang, Pengcheng; Yan, Bing; Gu, Guoqiang ; Yu, Zitong; Chen, Xi; Wang, Zengbo (James); Yang, Hui

Sensors and Actuators B: Chemical

DOI:
https://doi.org/10.1016/j.snb.2022.131401

Published: 15/04/2022

Peer reviewed version

Localized photonic nanojet based sensing platform for highly efficient signal amplification and quantitative biosensing

PengchengZhang[a1], BingYan[b1], GuoqiangGu[a], ZitongYu[a], XiChen[a], ZengboWang[b], HuiYang[a]

[a]Laboratory of Biomedical Microsystems and Nano Devices, Bionic Sensing and Intelligence Center, Institute of Biomedical and Health Engineering, Shenzhen Institute of Advanced Technology, Chinese Academy of Sciences, Shenzhen, China

[b]School of Computer Science and Electronic Engineering, Bangor University, Bangor, Gwynedd LL57 1UT, UK

Abstract

Light-analyte interaction systems are key elements of novel near-field optics based sensing techniques used for highly-sensitive detection of various kinds of targets. However, it is still a great challenge to achieve quantitative analysis of the targets using these sensing techniques, since critical difficulties exist on how to efficiently and precisely introduce the analytes into the desired location of the near-field light focusing, and quantitatively measure the enhanced optical signal reliably. In this work, we present for the first time a localized photonic nanojet (L-PNJ) based sensing platform which provides a strategy to achieve quantitative biosensing via utilizing a unique light-analyte interaction system. We demonstrate that individual fluorescent microsphere of different sizes can be readily introduced to the light-analyte interaction system with loading efficiency more than 70%, and generates reproducible enhanced fluorescence signals with standard deviation less than 7.5%. We employ this sensing platform for fluorescent-bead-based biotin concentration analysis, achieving the improvement on the detection sensitivity and limit of detection, opening the door for highly sensitive and quantitative biosensing. This L-PNJ based sensing platform is promising for development of next-generation on-chip signal amplification and quantitative detection systems.

Keywords

Optical amplification, Quantitative biosensing, Microsphere lens, Localized photonic nanojet, Light-matter interaction

1. Introduction

The ability of confining and concentrating light energy into a very small volume permits the efficient delivering of high-intensity optical energy to the micro/nano analytes of interest. This leads to enhanced light–matter interactions and generates profound effect on the efficacy of various optical processes, such as emission enhancement and radiation pattern modulation of chromophores (i.e., fluorophores, fluorescent nanodiamonds and semiconductor quantum dots), and the increased scattering signal of molecules [1], [2]. Consequently, it enables the development of near-field optics based novel sensing techniques (NFO-sensing techniques), with extensive applications in precision bioassays [3], [4], biochemical sensors [5], [6] and surface enhanced spectroscopies [7], [8], [9].

The light-analyte interaction system as the functional component in the NFO-sensing techniques provides the area for the target recognition and signal amplification. It performs the key element as its target-capture efficiency, field intensity, and volume mode determines the performance (response time, sensitivity and throughput) of the NFO-sensing techniques. Conventional light-analyte interaction systems are widely performed on metal-based plasmonic structures including array of nanostructures or nanoparticles, by taking advantage of electromagnetic resonances on metals such as surface plasmon modes. These surface plasmon modes generate highly enhanced electromagnetic field (so called hot spot) which accommodates and supports the light-analyte interactions. However, metal-based plasmonic structures share common drawbacks such as intrinsic optical losses in metals, small mode volume and technically challenging nanofabrication processes, therefore hindering their practical applications. Recent research trends now offer new platforms for light-analyte interaction system via using dielectric optical microstructures including microbeads, microcylinder and others [10], [11], [12]. Compared with metallic structures, dielectric microstructures possess simple structure and almost no intrinsic absorption. Therefore, utilization of dielectric microstructures is considered as a simple and cost-effective route for NFO-sensing techniques without requiring expensive nanofabrication facilities or complex near-field configurations [12], [13]. Upon illumination with the light, dielectric microstructures such as dielectric microbeads can modulate the spatial structure of the incident light and converge it into a concentrated light flux, which is termed as a “photonic nanojet” (PNJ). As the light is confined, its local field intensity can reach a value that is orders of magnitude higher than the incident intensity. Consequently, objects in the focus zone of the PNJ experience an enhanced electromagnetic excitation which stimulates strong light–matter interactions. This has brought the development of dielectric microstructures based optical techniques to various applications including super resolution

imaging [14], [15], ultrasensitive optical detection [16], [17], [18], [19], [20], optical trapping and manipulation [21], [22], [23].

However, it is still a great challenge to achieve quantitative analysis of the targets utilizing dielectric microstructures based NFO-sensing techniques, because PNJ is inherently a near-field phenomenon with relatively small effective volume and only analytes located within the PNJ make a significant contribution to the overall signal. Therefore, analytes are typically required to be coated into a film beneath the dielectric microstructures, with only a small fraction of analytes that coincidently in the converging area can be illuminated to participate in the light–matter interactions [19], [20]. Especially, the above described limitation is greatly hindering the possible applications of this approach in general for biosensing applications, where the biological analytes are always in small volume, low concentration, or possess uneven size distributions or fragile tissues, which are not capable of uniformly coating. Furthermore, due to the heterogeneous distribution on the intensity of the PNJ, signals that report the strength of light–analyte interaction could exhibit server fluctuations when spatial location of the analyte varies [24], [25]. This poses great challenges on achieving reliable signal amplification and obtaining accurate measurements and quantification as desired.

Here in this study, we present for the first time a localized PNJ based sensing platform which achieves highly efficient signal amplification and quantitative biosensing. The sensing platform consists of microwell-decorated microsphere lens (μ-well lens) array. Different from the conventional dielectric microbeads which generate PNJs in an open space, these μ-well lenses generate PNJs in a localized semi-open microwell, which is termed as localized PNJ (L-PNJ) here. The semi-open microwell allows passive trapping of single microscale analyte into the L-PNJ with high degree of spatial accuracy (Scheme 1). The novel design greatly improves the efficiency of introducing the targets into the L-PNJ as well as suppresses their signal fluctuations, allowing reliable measurement of signals amplified by enhanced light–matter interactions. This paves the way to establish a versatile and highly sensitive quantitative sensing platform. We demonstrate that fluorescent microspheres of different sizes can be efficiently introduced into the desired L-PNJ area and their location in the L-PNJ can be readily controlled and adjusted. Consequently, their fluorescent signals are amplified by the unique design due to the enhanced light–matter interactions within the L-PNJ. Therefore, the fluorescent enhancement factor, which reports the strength of light–matter interactions between the fluorescent microsphere and L-PNJ, can be reliably and accurately measured. Furthermore, we employ this μ-well lens array on fluorescence-based target analyte concentration analysis, by using biotin as a model sample, achieving the

improvement on detection sensitivity and limit of detection, demonstrating the ability of quantitative and sensitive detection of targets.

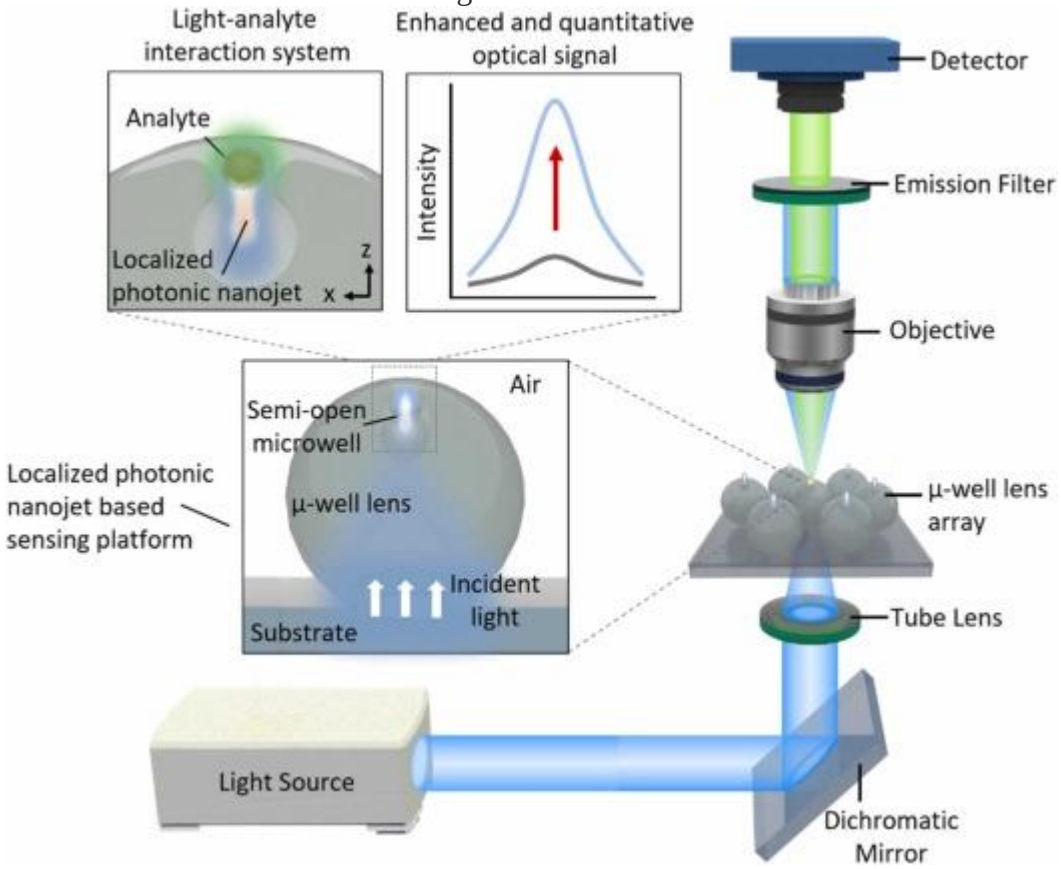

Scheme 1. Schematic illustration of the localized photonic nanojet based sensing platform and the experimental setup designed for quantitatively recording the fluorescent signal from the analytes in the light-analyte interaction system. Individual fluorescent microsphere is loaded in the semi-open microwell (light-analyte interaction system). Upon illumination from the bottom of the μ-well lens, localized photonic nanojet is generated inside the semi-open microwell, which excites the fluorescent microsphere and induces enhanced light–matter interactions, leading to the emission signal amplification. The emission signal is collected from the top via transmissive optical configuration.

2. Experimental section

2.1. Materials and regents

Barium titanate glass (BTG) microspheres were purchased from Cospheric Co., Santa Barbara, United States. Polydimethylsiloxane (PDMS, SYLGARD 184) was purchased from DOW CORNING, United States. Fluorescent microspheres (1 μm, 5 μm, 10 μm and 15 μm in diameter, respectively) dyed with fluorophores (475 nm in excitation and 525 nm in emission) and streptavidin conjugated polystyrene microspheres (5 μm in diameter) were purchased from So-Fe biomedicine Co., Shanghai, China. Cy3 dye (550 nm in excitation and

568 nm in emission) labeled biotin was purchased from GENEWIZ Co., Suzhou, China. Tween20 and PBS buffer (1X) was purchased from Sigma-Aldrich Co., China. Milli-Q water was used for all experiments. All the regents were used as received.

2.2. Fabrication of the μ-well lens array

BTG microspheres (refractive index=1.9) with size of ~80 μm were placed on a PDMS spin-coated glass substrate. The BTG microspheres were then gently spread over the substrate to form a monolayered microsphere array. The prepared sample was then processed by a nanosecond pulse laser (LMT2010P, Chongqing Yongmao Machinery and Electronics Co., Ltd, central wavelength $\lambda = 1064$ nm, pulse duration 100 ns, pulse power up to 10 w). The laser beam was incident from the backside of the glass substrate and passed through the microsphere. Due to the high refractive index of BTG microsphere, the laser beam passing through microspheres can undergo a second focusing, generating a highly localized hot spot at the boundary. This optical phenomenon, also known as a "photonic nanojet", creates intensively localized energy at the boundary that causes the material to be removed. Finally, a semi-open microwell was formed at the dark side of each microsphere.

2.3. Modification of the biotin conjugated polystyrene microsphere

70 μL streptavidin conjugated polystyrene microspheres (10 mg/ml) was aliquoted into 7 × 10 μL in centrifuge tubes. Cyanine3 (Cy3) dye labeled biotin was dissolved in 100 μL 1 ×PBS buffer into concentrations of 100 μM, 10 μM, 1 μM, 100 nM, 10 nM, 1 nM, 0.1 nM, respectively. Subsequently, the Cy3 dye labeled biotin with different concentrations were added into the tubes each with 10 μL streptavidin conjugated polystyrene microspheres, respectively. The mixtures were allowed to react at 37 ℃ for 30 min away from light in a shaker. The mixtures were then centrifuged and washed twice with PBST buffer (1 ×PBS buffer with 0.05% Tween20). Finally the precipitations were dissolved in 100 μL Milli-Q respectively for further experiments.

2.4. Loading fluorescent microspheres in the semi-open microwell by self-assembly

The chip with μ-well lenses was cleaned with 2-proponal, rinsed with Milli-Q water and dried with nitrogen. Afterwards, air plasma was used to treat the chip for 1 min to increase the surface hydrophilicity of the μ-well lenses. Subsequently, 10 μL of the fluorescent microspheres ($\sim 1.5 \times 10^6$ ml^{-1}) in Milli-Q water was dropped on the chip. The droplets spread out over the whole surface area due to the hydrophilicity of the surface. The evaporation of the liquid was then benefited. During the end of the liquid evaporation, curved meniscus existed from liquid to microsphere surface. This induces capillary forces and drives these fluorescent microspheres close into the semi-open microwell [26], [27]. After gently

washed with Milli-Q water, fluorescent microspheres left around the corner of the μ-well lenses are washed away and eventually only microspheres in the semi-open microwells are remained. Then the chip was dried for further characterization. It should be noted that, unbalanced capillary force during evaporation or the electrostatic force may cause some small fluorescent microspheres (<10% for fluorescent microspheres of 1 μm and 5 μm) randomly adhere to the inner surface of the semi-open microwells. Therefore, an off-center position occurred for these fluorescent microspheres. They can be distinguished by measuring their geometric positions in the μ-well or by reading their focal lengths. They are excluded from the statistics. Such phenomenon is rarely observed on fluorescent microspheres located outside the semi-open microwell (fluorescent microspheres of 10 μm and 15 μm), largely due to the strong self-complementary key-lock mechanisms with the "neck" of the semi-open microwell.

2.5. Recording and measuring fluorescent signal under the light microscope

The samples were characterized under the light microscope (Zeiss Axio Observer 7) equipped with a 10 × objective with NA= 0.25 and a 40 × objective with NA= 0.55. The sample was placed upright on the sample stage. The 40 × objective was used to observe the topography of the sample. During the emission collection process, the excitation light was illuminated from the bottom of the sample and the 10 × objective lens was used to collect the emission signal above the sample, as illustrated in Scheme 1. For the fluorescent microspheres in the microwells or on the substrate, the objective lens was focused on the fluorescent microspheres when collecting the signal. In brief, the objective was firstly focused on the outer contour of the fluorescent microspheres and then was adjusted to the focal length where the recorded fluorescence intensity reaches the maximum.

3. Results and discussion

3.1. Fabrication and characterization of the μ-well lens array

Conventional BTG dielectric microspheres are utilized and the fabrication of μ-well lens array is illustrated in Fig. 1a. Upon illumination with a plane wave (wavelength $\lambda = 1064$ nm) from the bottom, simulation based on Mie calculations show that a focused high-intensity beam, i.e., PNJ, is generated on the top surface of the BTG microsphere (Fig. S1). The high-intensity PNJ can generate heat that enables ablation and direct removal of BTG material in the focal area due to the thermal accumulation effect, leading to the formation of a semi-open microwell [28].

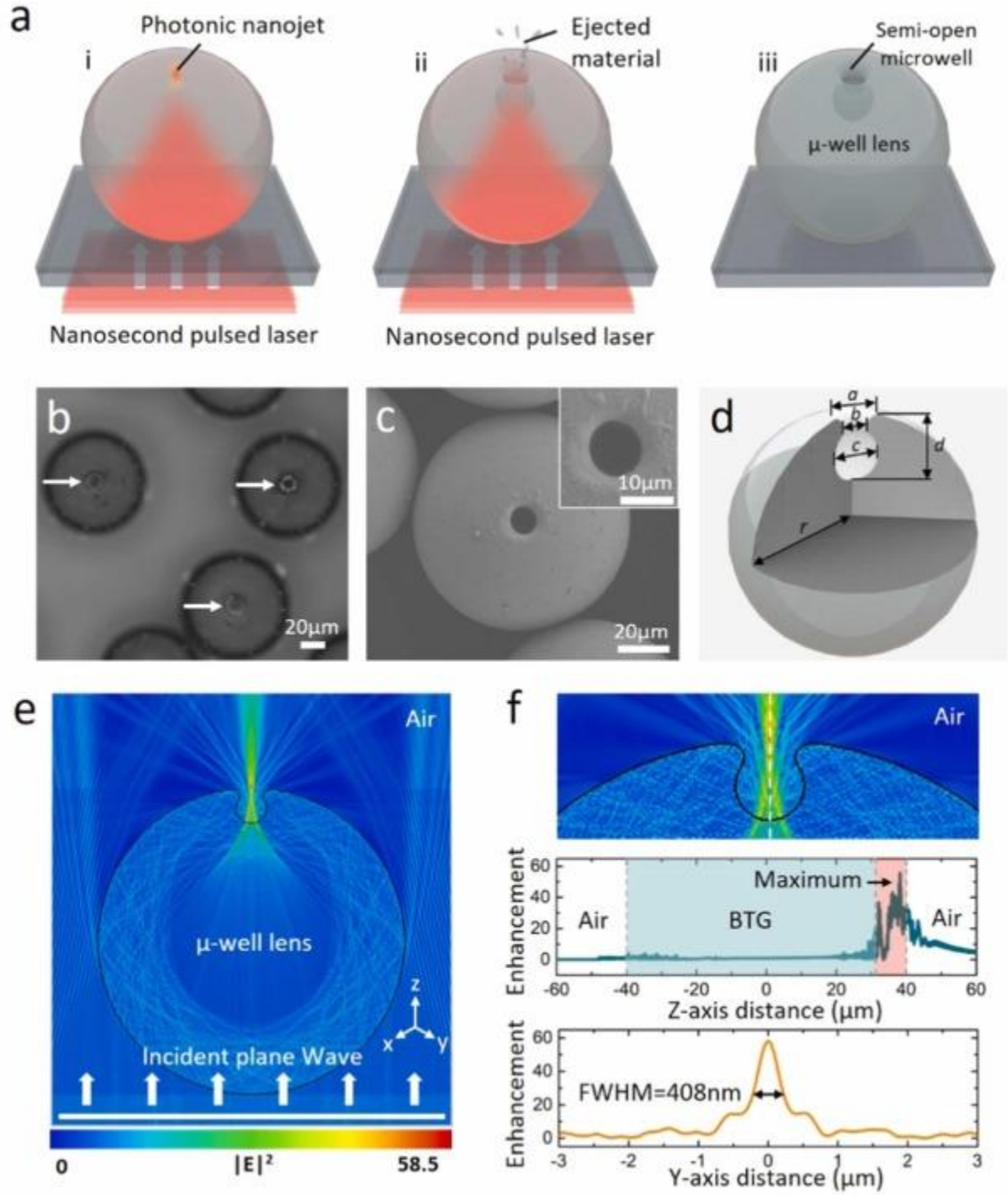

Fig. 1. Fabrication and characterization of the μ-well lens. (a) Schematic illustration of the fabrication process of the semi-open microwell in the BTG microspheres. (b) Photographic image of the as-prepared BTG microspheres with semi-open microwells. The white arrows indicate the semi-open microwells on each BTG microsphere. (c) Scanning electron microscope (SEM) image of the as-prepared μ-well lens. (d) Schematic illustration on the dimensions of the fabricated μ-well lens. (e) Simulation based on finite-difference time-domain showing localized PNJ can be generated inside the semi-open microwell. (f) Plot of the electric field intensity distribution along z-axis and FWHM of the PNJ. The white, green and pink areas in

the middle image represent the area of air, BTG material and semi-open microwell, respectively. (For interpretation of the references to colour in this figure legend, the reader is referred to the web version of this article.)

The as-prepared μ-well lens is characterized under light microscope, as shown in Fig. 1b. These semi-open μ-well can be clearly observed under light microscope since they exhibit dark circular area on the top center of each μ-well lens. The scanning electron microscopy (SEM) images under high magnification show that a larger outer contour of about 11 μm is on the top of the BTG microsphere, Fig. 1c. The radius of this outer contour gradually shrinks and eventually narrows into a semi-open microwell with a diameter of about 6 μm. Besides, the interior of the μ-well is observed to be an ellipsoidal cavity which shows a maximum cross-sectional profile of about 13 μm and a height of about 20 μm, as illustrated in Fig. 1d. Further details on the interior and cross-section of the semi-open microwells are presented in supporting information (Fig. S2). The size of the semi-open microwell can be controlled via tuning the power of the nanosecond laser beam and the number of laser exposure times during the fabrication process. Utilization of ultrafast laser, such as picosecond or femtosecond laser, would benefit the fabrication of semi-open microwells down to sub-micron scale.

Simulation based on finite-difference time-domain (FDTD) is performed to investigate the optical focusing property of the as-prepared μ-well lens in air ambient (Fig. 1e). The simulation shows that, upon illumination from the bottom, the incident light (plane wave with wavelength $\lambda = 475$ nm, which is the excitation central wavelength of the fluorescent samples used later) can be converged and a PNJ is generated and confined inside the semi-open microwell, which is termed as localized photonic nanojet (L-PNJ). Besides, the maximum of the electric field occurs inside the semi-open microwell and the lateral resolution of the L-PNJ (FWHM) is 408 nm, as shown in Fig. 1f. It should be noted that, PNJs are usually developed in a less controlled open space for the ordinary microsphere or microcylinder structure, which makes it technically difficult to accurately introduce target into this space. Current solutions such as random capture based on microfluidics or manual trapping by optical forces severely hinder sample throughput and require complex experimental configurations [18], [22]. As a comparison, the additional semi-open microwell in our μ-well lens provides the ability to further confine the PNJ into a restricted space, leading to a more accurate way to locate the object and to detect signal from the object. This creates a decent light-analyte interaction system and once the target is loaded into the semi-open microwell, it can be simultaneously illuminated by the high-intensity L-PNJ without any further manipulations.

3.2. Performance on the passive trapping of fluorescent microspheres into the light-analyte interaction system

To demonstrate the microscale objects trapping capabilities of the light-analyte interaction system, as well as measuring the signal boosted by enhanced light–matter interactions, fluorescent microspheres in aqueous dispersion are utilized. Previous studies have shown that substrates patterned by concave features possess local energy minima which can efficiently trap particles by employing self-complementary key-lock mechanisms in the solution during the assembly process [29]. Similarly, here we demonstrate that owing to the localized area provided by this μ-well lens, the particles as target in dispersion can be passively trapped into the μ-well lens driven by the capillary force as the solvent gradually evaporates. Fluorescent microspheres with diameter of 1 μm, 5 μm, 10 μm and 15 μm are utilized in the experiments, respectively. The passively trapping process is illustrated in Fig. 2a. The recessed circular geometry of the semi-open microwell benefits the onset of self-complementary key-lock mechanisms between sample microspheres and the semi-open microwells. Together with van der Waals, or depletion forces, fluorescent microspheres are confined and irreversibly trapped in the semi-open microwells. Loading efficiency is used to quantify the effect of passively trapping process. It is defined as the ratio of the number of the microwells containing the fluorescent microspheres to the total number of the microwells in a statistical area. We perform multiple loading steps (each loading process in Fig. 2a is referred to as one step) and find that the loading efficiency depends on the number of loading steps and the size of fluorescent microspheres, Fig. 2b. The loading efficiency increases as the number of loading steps increases. Typically, these semi-open microwells can be filled at a yield above 70% after 5 loading steps for all the fluorescent microspheres used in our experiments. However, given the same number of loading steps and the concentration of dispersion, higher loading efficiency is observed for smaller fluorescent microspheres. The size-dependent loading efficiency is ascribed to the size induced loading preference during the assembly process [30], [31]. The fluorescent microspheres with smaller size encounter higher possibilities to be trapped and meanwhile possess higher stability in the semi-open microwells, inducing higher loading efficiency compared with those with larger size. Multiple fluorescent microspheres in a single semi-open microwell or under the μ-well lenses will bring interference on the quantitative determination of fluorescent signals in the following experiments. To reduce this interference, it is necessary to load only a single microsphere in each single semi-open microwell. This can be achieved by employing a diluted dispersion in the self-assembly process and performing more loading steps. Here, samples with a single microsphere loaded in a single semi-open microwell are used as the

sample group and individual fluorescent microspheres distributed on the substrate are chosen as the control group.

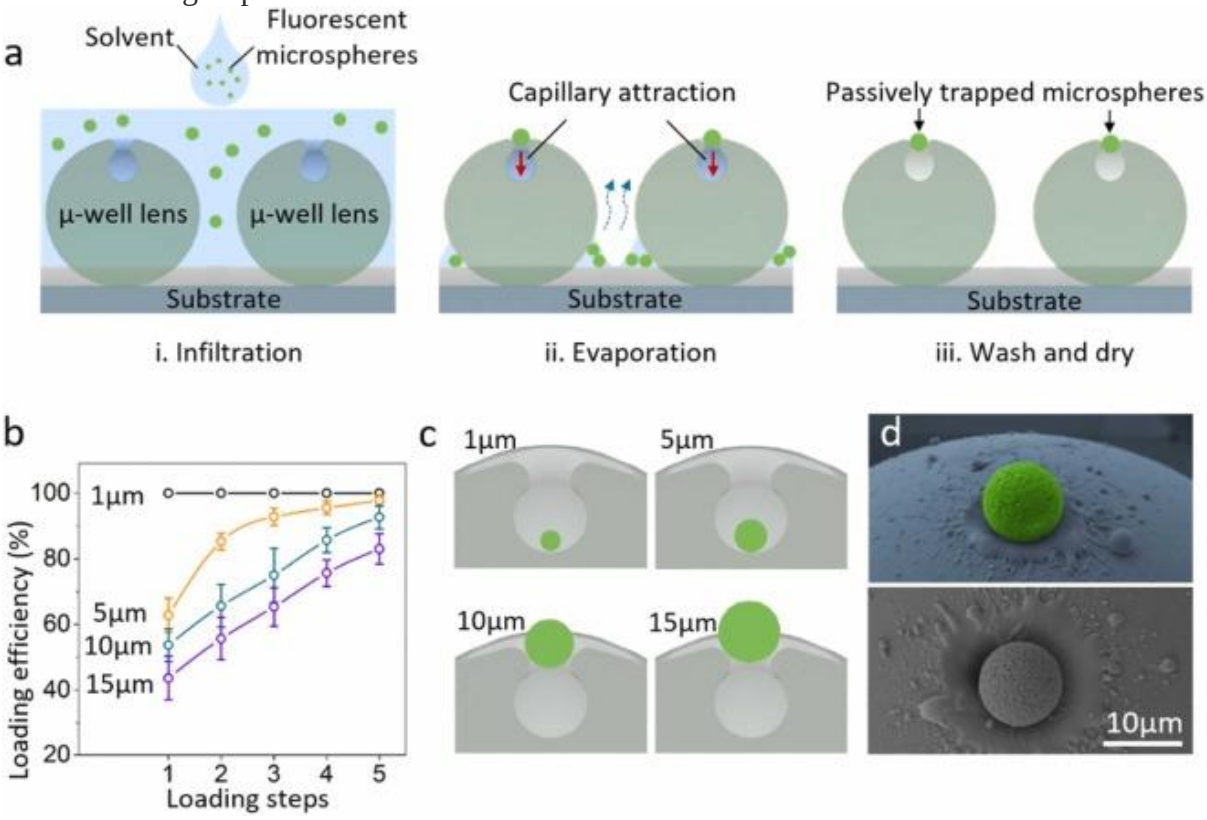

Fig. 2. (a) Schematics depicting the process of the fluorescent microsphere trapping capability of the μ-well lens. (b) Dependency of the loading efficiency on the number of loading steps. The full lines represent guides to the eye. (c) Schematic illustration of the positions of fluorescent microspheres with different sizes loaded in the semi-open microwell. (d) SEM images showing the fluorescent microsphere of 10 μm located in the semi-open microwell. Upper: side view of the false color SEM image; Lower: top view of the SEM image. (For interpretation of the references to colour in this figure legend, the reader is referred to the web version of this article.)

Once the L-PNJ is generated, the trapped microspheres in the semi-open microwell are automatically exposed in the enhanced electromagnetic field and no further manipulation is required. It should be noted that, these fluorescent microspheres can exhibit different height distributions along the longitudinal direction, Fig. 2c. Fluorescent microspheres (1 μm and 5 μm) with diameter smaller than the “neck” of the semi-open microwell (value b in Fig. 1d) enter the semi-open microwell while others (10 μm and 15 μm) are blocked and located outside the semi-open microwell. The SEM images shown in Fig. 2d confirm that, after the evaporation of solvent, individual fluorescent microsphere with diameter of 10 μm is targeted by the μ-well lens of the light-analyte interaction system.

The loading strategy here provides a simple yet effective approach to introduce the individual microsphere into the L-PNJ with controlled position. Besides, the self-complementary key-lock mechanisms enables the physical contact between microspheres and the semi-open microwells. Thus, the spatial variations of the microsphere in the semi-open microwell are highly reduced. As a result, microspheres of the same size are located at the same height along the longitudinal direction and thus experience nearly identical intensity of the L-PNJ, leading to suppressed signal fluctuation. This light-analyte interaction system benefits the reliable measurement of signals boosted by enhanced light–matter interactions and enables its application in quantitative detection.

3.3. Highly efficient optical signal amplification and reliable signal quantification via measuring the fluorescent enhancement factor in the light-analyte interaction system

After the fluorescent microspheres are loaded, their fluorescent signal is recorded in the air ambient under the light microscope as illustrated in Scheme 1. The excitation light (central wavelength $\lambda = 475$ nm) is incident from the bottom of the μ-well lens, inducing L-PNJ in the semi-open microwell on the top. The emission light (central wavelength $\lambda = 525$ nm) from the fluorescent microsphere is collected by an objective (10 ×, numerical aperture NA = 0.25) above the sample. To prove the optical enhancement provided by this μ-well lens, the emission light from the fluorescent microspheres on the substrate is also collected with the identical excitation power and exposure time as a control, as illustrated in Fig. 3a. As expected, fluorescent microspheres inside the semi-open microwells exhibit higher emission intensity than those on the substrate, as shown in Figs. 3b and S4. Bright visible emission is observed for the fluorescent microspheres inside the semi-open microwells, while only inconspicuous emission is captured for those on the substrate. Their fluorescent intensity curve of the corresponding fluorescent microspheres is shown in Fig. 3c. The signal amplification effect in the light-analyte interaction system can be clearly observed as the fluorescent microspheres in the semi-open microwell (green curve) exhibits higher intensity than the control sample (orange curve).

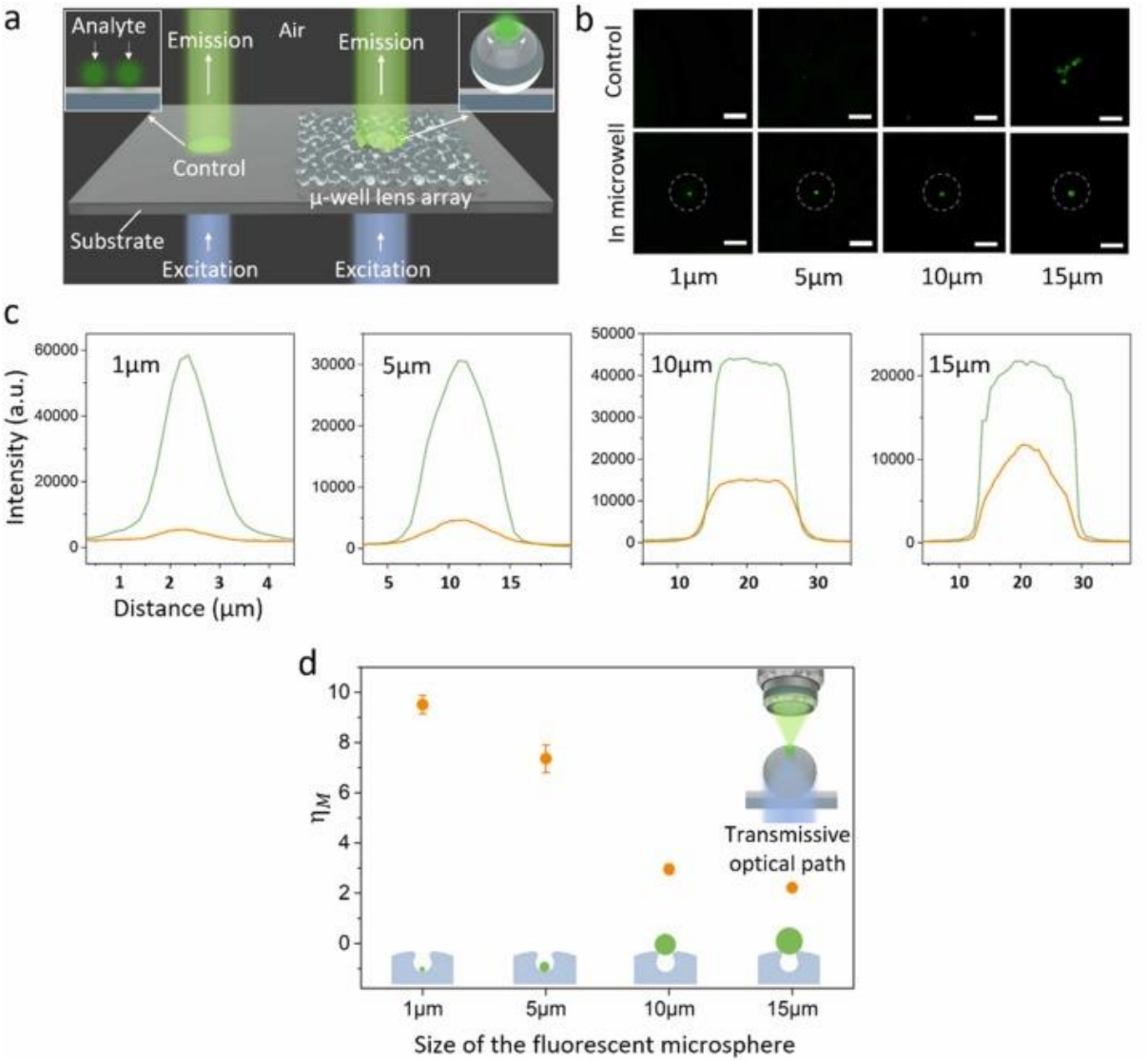

Fig. 3. (a) Schematic illustration of the signal recording for the fluorescent microspheres in the semi-open microwells and on the substrate (control) and (b) corresponding recorded fluorescent signals. (c) The fluorescent intensity from the corresponding fluorescent microspheres showing the enhanced fluorescent signal (green curve) and the control signal (orange curve). (d) The enhancement factor v.s. the size of the fluorescent microspheres measured by experiment (error bar stands for standard deviation).

To quantify the signal amplification effect of this light-analyte interaction system, we define mean emission intensity enhancement factor ηM as(1)$\overline{\eta}$M=Iμ$\overline{I}$cwhere $\overline{I}$μrepresents the arithmetic mean emission intensity of the fluorescent microspheres when positioned inside the semi-open microwells and $\overline{I}$c represents the arithmetic mean emission intensity of the fluorescent microspheres on the glass substrate (control). The measured magnitude of ηM reflects the optical enhancement capability of this light-analyte interaction system, while the measured standard deviation (SD) represents the signal fluctuation, i.e., the stability

of the enhanced emission signal (shown as error bar in plot). We repeated measurements of ηM for different sized fluorescent microspheres at different locations, and statistical results were shown in Fig. 3d. Note the detected emission signal from individual fluorescent microsphere presented here was randomly selected, and consistent uniformity can be found for all the fluorescent microspheres with the same size. Overall, the fluorescent signal turned to be quite stable for all measured cases, with SD all below 7.5%. This in turn suggests the developed μ-well systems are overall stable and reliable for precision measurement of micro/nanoscale signals. A slightly larger SD values were observed for smaller particles of sizes 1 μm and 5 μm, when compared to 10 μm and 15 μm sized particle. This is caused by the fact that smaller fluorescent particles are more likely to be deposited at different locations inside the microwell (Section 2.4 in experimental section). On the other hand, Fig. 3d also shows that the enhancement factor ηM decreases with particles sizes. For instance, up to one order (about 9.5-fold) of enhancement was obtained for the fluorescent microsphere of 1 μm, about 2-fold of enhancement for that of 15 μm. Since differently sized fluorescent microspheres could be trapped at different z-locations in the microwell, it would lead to a general 'size effect' on the enhancement factor for the fluorescent signal, i.e., the smaller the particle size, the higher the enhancement factor. The focusing L-PNJ inside microwell (FWHM = 408 nm, see Fig. 1f) is in comparable size to fluorescent microspheres of 1 μm, but smaller than other size of fluorescent microspheres of 5 μm, 10 μm and 15 μm. This suggests for larger particles the PNJ doesn't provide a full illumination of the particle, but only partially. The excitation of fluorescence molecules will be limited to the excited regions determined by PNJ (i.e., similar level of input energy) while the emitted fluorescent light will distribute through the whole sphere (i.e., larger area output). This will cause a reduced average intensity and thus a lower enhancement factor as observed in experiments.

3.4. Mechanism accounting for the signal amplification in the light-analyte interaction system

Apart from creating the L-PNJ with high excitation field intensity, this light-analyte interaction system can also enhance the efficiency of far-field light collection and in turn contribute to the fluorescent enhancement factor. As indicated from the results of dipole scattering FDTD simulation, in the absence of the μ-well lens, a dipole source is radiating energy uniformly into its surrounding space (Fig. 4a). However, in Fig. 4b, one can see the μ-well lens significantly changes the radiation directivity of the dipole source and redirects the energy mostly toward the top (90-deg angle) and bottom directions (270-deg angle) of the lens, leading to significant increase in signal collection efficiency. The calculating results show that the light-analyte interaction system leads to an around 14% increase on the mean collection efficiency upon collecting from 90-deg angle (Fig. S6). Based on these results, the

light-analyte interaction system increases the detected mean emission intensity by inducing high-intensity L-PNJ, while at the same time it provides an enhanced collection efficiency by redirecting the radiation pattern. By combining these two effects, the mean emission intensity enhancement factor ηM is expressed as the synergistic effect of field enhancement and collection efficiency on the optical enhancement as following,(2)ηM=ηcol·ηexcwhere ηcol representing the enhancement on the collection efficiency and ηexc representing the enhancement factor on the excitation intensity arising from the high-intensity PNJ. A simple model is developed to explain how the ηM evolves with the size of the fluorescent microspheres. The calculated ηM from the model fits well with the trends obtained from the experiments. Details on the theoretical model is presented in the section 9 in the supporting information.

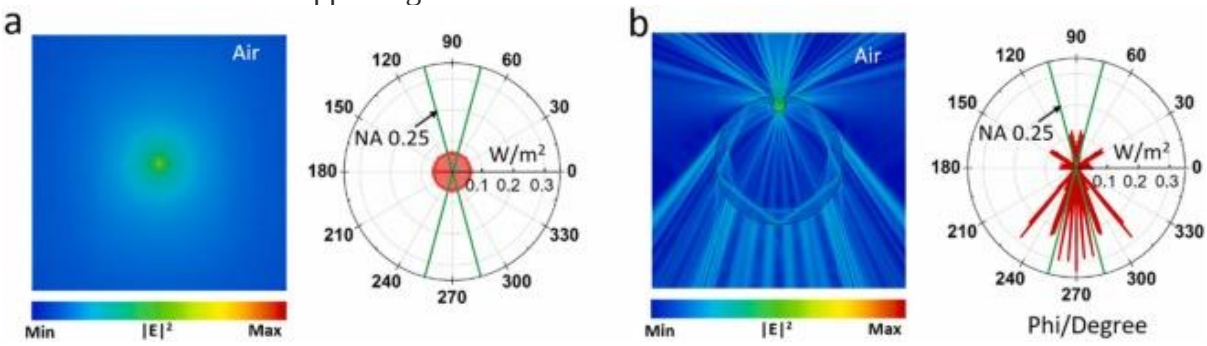

Fig. 4. Simulations based on FDTD showing the far-field emission collection efficiency for a dipole source obtained on the absence (a) and in the presence (b) of the μ-well lens (left image) and the corresponding radiation pattern (right image) respectively. The dipole is in a free space for (a) and is set on the bottom of the semi-open microwell for (b). The crossed green lines indicate the light collection area under the objective with NA of 0.25 used in our experiments.

3.5. Quantitative biotin concentration analysis utilizing L-PNJ based sensing platform

As one of the possible practical applications of this L-PNJ based sensing platform with the capability of signal quantification, we further demonstrate a fluorescent bead-based quantitative biotin concentration analysis. Polystyrene (PS) microspheres of 5 μm are modified with Cyanine 3 (Cy3) dye labeled biotin with different concentrations, ranging from 100 μM down to 100 pM, as illustrated in Fig. 5a. Fluorescent signal at the focal plane of the modified PS microspheres in the semi-open microwell and on the glass substrate is collected under TR configuration. The corresponding recorded fluorescent images in concentration of 100 μM and 10 nM are shown in Fig. 5b, respectively. It is shown that utilization of this novel μ-well lens increases the fluorescent intensity of the modified PS microspheres. Meanwhile, the fluorescent intensity under different concentration of biotin is shown in Fig.

5c. It is observed that, the fluorescence intensity of the PS microspheres located in the semi-open microwell is higher than that in the absence of the μ-well lens at each concentration. Note that the relatively large standard deviation in Fig. 5c is ascribed to the relatively large intrinsic fluorescent variation on the modified PS microspheres compared to the commercial fluorescent microspheres. The higher slope extracted from Fig. 5c for the PS microspheres in the semi-open microwell implies an increase (about 1.8-fold) in the sensitivity of biotin response upon signal amplification. Moreover, the amplification on the fluorescent signal improves the signal-to-noise ratio (SNR) and enables a lower limit of detection (LOD). For instance, at a concentration of 0.1 nM (corresponding to 0.024 ng/ml), fluorescent signal amplified by the μ-well lens is still detectable with SNR= 9.0, while the fluorescent signal without amplification cannot be distinguished from the background noise. By assuming a linear relationship between the fluorescent intensity and the concentration of the biotin (in logarithmic scale), we can deduce a LOD of 35 pM (corresponding to 8.6 pg/ml) with SNR= 3.0 upon signal amplification. Therefore, the utilization of our novel μ-well lens for signal amplification improved both the detection sensitivity and the LOD.

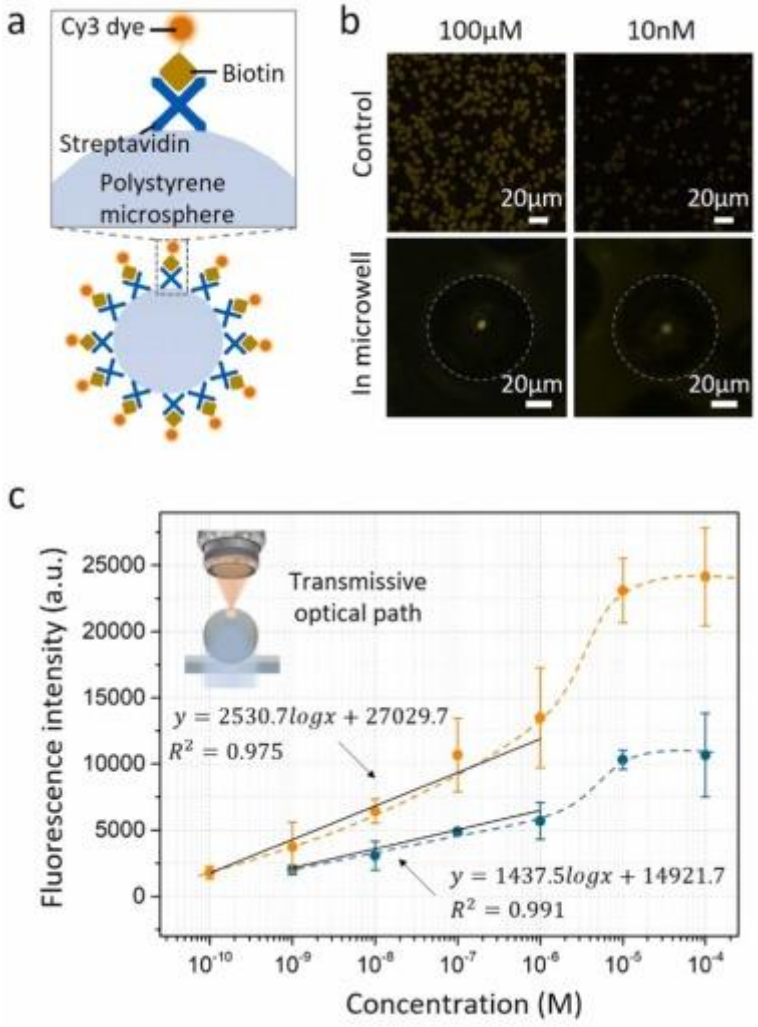

Fig. 5. (a) Schematic illustration of the Cy3-labeled polystyrene (PS) microspheres. (b) Recorded fluorescent signals of the fluorescent dye-labeled PS microspheres in the semi-open microwells and on the substrate (control). (c) Recorded fluorescent intensity in different concentrations of biotin under transmissive optical configuration. The orange and blue dots represent the intensity recorded with and without fluorescent signal amplification, respectively. The dashed lines represent guides to the eye. The solid black lines represent the linear regression curves of the corresponding data. The linear regression equations are also shown, respectively.

4. Conclusion

Method of developing reliable optical enhancement and achieving accurate signal quantification through PNJ based NFO-sensing techniques is previously undescribed. In this work, we have taken an important step in validating the L-PNJ based sensing platform by employing a dielectric microsphere based μ-well lens. We have demonstrated that L-PNJ can be generated in a semi-open microwell and thus creates a decent light-analyte interaction system. Individual fluorescent microsphere of different sizes can be introduced to the designated position in the L-PNJ with an efficiency more than 70% and generates reproducible enhanced fluorescence signals with standard deviation smaller than 7.5%. This has led to reliable optical enhancement and quantitative signal measurements. In addition, a comprehensive analysis on the optical properties of this μ-well lens reveals the mechanism accounting for the signal amplification in the light-analyte interaction system. This L-PNJ based sensing platform is employed on biotin concentration analysis, achieving a 1.8-fold increase in sensitivity and also the improvement on limit of detection. This sensing platform is promising for development of next-generation on-chip signal amplification and quantitative detection systems as well as for investigating a wide range of light–matter interaction processes.

Credit authorship contribution statement

H.Y. and Z.W. supervised the project. B.Y. prepared the μ-well lens sample; P.Z. conceived the study and designed the experiments; P.Z., Z.Y., X.C. and G.G. performed the experiments; B.Y. conducted the simulation; P.Z. analyzed the data; P.Z. and B.Y. wrote the manuscript; H.Y. and Z.W. edited the manuscripts.

Declaration of Competing Interest

The authors declare that they have no known competing financial interests or personal relationships that could have appeared to influence the work reported in this paper.

References

[1] J.A. Schuller, E.S. Barnard, W. Cai, Y.C. Jun, J.S. White, M.L. Brongersma, Plasmonics for extreme light concentration and manipulation, Nat. Mater., 9 (2010), pp. 193-204

[2] S. Yan, J. Chen, L. Cai, P. Xu, Y. Zhang, S. Li, P. Hu, X. Chen, M. Huang, Z. Chen, Light-matter interaction within extreme dimensions: from nanomanufacturing to applications, Adv. Opt. Mater., 6 (2018), Article 1800444

[3] S. Schultz, D.R. Smith, J.J. Mock, D.A. Schultz, Single-target molecule detection with nonbleaching multicolor optical immunolabels, Proc. Natl. Acad. Sci. USA, 97 (2000), pp. 996-1001

[4]J.M. Nam, C.S. Thaxton, C.A. Mirkin, Nanoparticle-based bio-bar codes for the ultrasensitive detection of proteins, Science, 301 (2003), pp. 1884-1886

[5] J.N. Anker, W.P. Hall, O. Lyandres, N.C. Shah, J. Zhao, R.P. Van Duyne, Biosensing with plasmonic nanosensors, Nat. Mater., 7 (2008), pp. 442-453

[6] A.M. Armani, R.P. Kulkarni, S.E. Fraser, R.C. Flagan, K.J. Vahala, Label-free, single-molecule detection with optical microcavities, Science, 317 (2007), pp. 783-787

[7] H. Im, K.C. Bantz, S.H. Lee, T.W. Johnson, C.L. Haynes, S.H. Oh, Self-assembled plasmonic nanoring cavity arrays for SERS and LSPR biosensing, Adv. Mater., 25 (2013), pp. 2678-2685

[8] S.C. Luo, K. Sivashanmugan, J.D. Liao, C.K. Yao, H.C. Peng, Nanofabricated SERS-active substrates for single-molecule to virus detection in vitro: a review, Biosens. Bioelectron., 61 (2014), pp. 232-240

[9] K.J. Yi, H. Wang, Y.F. Lu, Z.Y. Yang, Enhanced Raman scattering by self-assembled silica spherical microparticles,J. Appl. Phys., 101 (2007), Article 063528

[10] Z. Chen, A. Taflove, V. Backman, Photonic nanojet enhancement of backscattering of light by nanoparticles: a potential novel visible-light ultramicroscopy technique, Opt. Express, 12 (2004), pp. 1214-1220

[11] X. Li, Z. Chen, A. Taflove, V. Backman, Optical analysis of nanoparticles via enhanced backscattering facilitated by 3-D photonic nanojets, Opt. Express, 13 (2005), pp. 526-533

[12]B.S. Luk'yanchuk, R. Paniagua-Domínguez, I. Minin, O. Minin, Z. Wang, Refractive index less than two: photonic nanojets yesterday, today and tomorrow [Invited],Opt. Mater. Express, 7 (2017), p. 18[13]

[13] A. Heifetz, S.C. Kong, A.V. Sahakian, A. Taflove, V. Backman,Photonic nanojets,J. Comput. Theor. Nanosci., 6 (2009), pp. 1979-199220

[14] Z. Wang, W. Guo, L. Li, B. Luk'yanchuk, A. Khan, Z. Liu, Z. Chen, M. Hong

Optical virtual imaging at 50 nm lateral resolution with a white-light nanoscope

Nat. Commun., 2 (2011), p. 218

[15] H. Yang, N. Moullan, J. Auwerx, M.A.M. Gijs, Super-resolution biological microscopy using virtual imaging by a microsphere nanoscope Small, 10 (2014), pp. 1712-1718

[16] D. Gérard, A. Devilez, H. Aouani, B. Stout, N. Bonod, J. Wenger, E. Popov, H. Rigneault, Efficient excitation and collection of single-molecule fluorescence close to a dielectric microsphere, J. Opt. Soc. Am. B, 26 (2009), pp. 1473-1478

[17] P. Ghenuche, J. de Torres, P. Ferrand, J. Wenger, Multi-focus parallel detection of fluorescent molecules at picomolar concentration with photonic nanojets arrays, Appl. Phys. Lett., 105 (2014), Article 131102

[18] H. Yang, M. Cornaglia, M.A. Gijs, Photonic nanojet array for fast detection of single nanoparticles in a flow, Nano Lett., 15 (2015), pp. 1730-1735

[19] L. Liang, D.B.L. Teh, N.D. Dinh, W. Chen, Q. Chen, Wu, Y. Wu, S. Chowdhury, A. Yamanaka, T.C. Sum, C.H. Chen, N.V. Thakor, A.H. All, X. Liu, Y,Upconversion amplification through dielectric superlensing modulation, Nat. Commun., 10 (2019), p. 1391

[20] K.A. Sergeeva, M.V. Tutov, S.S. Voznesenskiy, N.I. Shamich, A.Y. Mironenko, A.A. Sergeev Highly-sensitive fluorescent detection of chemical compounds via photonic nanojet excitation Sens. Actuators B Chem., 305 (2020), Article 127354

[21] Y. Li, H. Xin, X. Liu, Y. Zhang, H. Lei, B. Li， Trapping and detection of nanoparticles and cells using a parallel photonic nanojet array， ACS Nano, 10 (2016), pp. 5800-5808

[22] Y.C. Li, H.B. Xin, H.X. Lei, L.L. Liu, Y.Z. Li, Y. Zhang, B.J. Li Manipulation and detection of single nanoparticles and biomolecules by a photonic nanojet Light Sci. Appl., 5 (2016), Article e16176

[23] D. Lu, M. Pedroni, L. Labrador-Paez, M.I. Marques, D. Jaque, P. Haro-Gonzalez Nanojet trapping of a single sub-10 nm upconverting nanoparticle in the full liquid water temperature range Small, 17 (2021), Article e2006764

[24] W. Shen, X. Lin, C. Jiang, C. Li, H. Lin, J. Huang, S. Wang, G. Liu, X. Yan, Q. Zhong, B. Ren Reliable quantitative SERS analysis facilitated by core-shell nanoparticles with embedded internal standards Angew. Chem. Int Ed., 54 (2015), pp. 7308-7312

[25] S.E.J. Bell, G. Charron, E. Cortés, J. Kneipp, M.L. de la Chapelle, J. Langer, M. Procházka, V. Tran, S. Schlücker Towards reliable and quantitative Surface-Enhanced Raman Scattering (SERS): from key parameters to good analytical practice Angew. Chem., 59 (2020), pp. 5454-5462

[26] J. Jiang, J. Gao, H. Zhang, W. He, J. Zhang, D. Daniel, X. Yao Directional pumping of water and oil microdroplets on slippery surface Proc. Natl. Acad. Sci. USA, 116 (2019), pp. 2482-2487

[27] P. Peruzzo, A. Defina, H.M. Nepf, R. Stocker Capillary interception of floating particles by surface-piercing vegetation Phys. Rev. Lett., 111 (2013), Article 164501

[28] W. Wu, A. Katsnelson, O.G. Memis, H. Mohseni A deep sub-wavelength process for the formation of highly uniform arrays of nanoholes and nanopillars Nanotechnology, 18 (2007), Article 485302

[29] N.M. Silvestre, Q. Liu, B. Senyuk, I.I. Smalyukh, M. Tasinkevych Towards template-assisted assembly of nematic colloids Phys. Rev. Lett., 112 (2014), Article 225501

[30] M. Rycenga, P.H.C. Camargo, Y. Xia Template-assisted self-assembly: a versatile approach to complex micro- and nanostructures Soft Matter, 5 (2009), pp. 1129-1136

[31] P. Zhang, X. Chen, H. Yang Large-scale fabrication of photonic nanojet array via template-assisted self-assembly Micromachines, 11 (2020), p. 473